ELECTRON SPECTROSCOPY OF SURFACES

Elemental and Chemical Analysis with X-ray Photoelectron Spectroscopy

---

Versuch Nr. 35
F-Praktikum in den Bachelor- und Masterstudiengängen
Physik Department
Lehrstuhl E20, Raum 229

Contacts: Dr. Ignacio Piquero-Zulaica, PD Dr. Francesco Allegretti

---

1 Introduction

Photoelectron spectroscopy (PES) is one of the most established methods for determining the elemental composition and the chemical state of solid surfaces and thin films. This experiment focuses on **X-ray Photoelectron Spectroscopy** (**XPS**), which exploits X-ray photons to excite electrons from the core levels of the atoms of a solid into the vacuum, thus probing the electronic structure of matter with elemental sensitivity and chemical state specificity.

The purpose of the experiment is to make the students familiar with the fundamental principles and basic methodology of XPS, also offering an insight into the underlying physics. A number of different samples will be investigated in order to highlight the main information that the technique can provide and to show how XPS can be of relevance for a vast range of systems, not only in condensed matter physics, chemistry, and materials science, but also in applied physics and biophysics.
The technical basis of the experiment includes:

- basics of ultra-high vacuum technology
- generation of X-ray radiation
- analysis in energy and detection of electrons
- characterization of solid samples by XPS
- computer control of the measurements
- data analysis via computer software

Learning how to understand and interpret the experimental data and drawing up a short scientific report (in German or English) are further achievements of this FOPRA experiment. The experimental session will typically last about five hours and will be followed by a colloquium a few days after handing in the report.

2 X-ray Photoelectron Spectroscopy

2.1 Underlying physical principles and fundamental aspects

XPS is based, in principle, on a very simple process. When a solid surface is irradiated with soft X-ray photons (Fig. 1a), an incident photon of energy $\hbar\omega$ can be absorbed by an

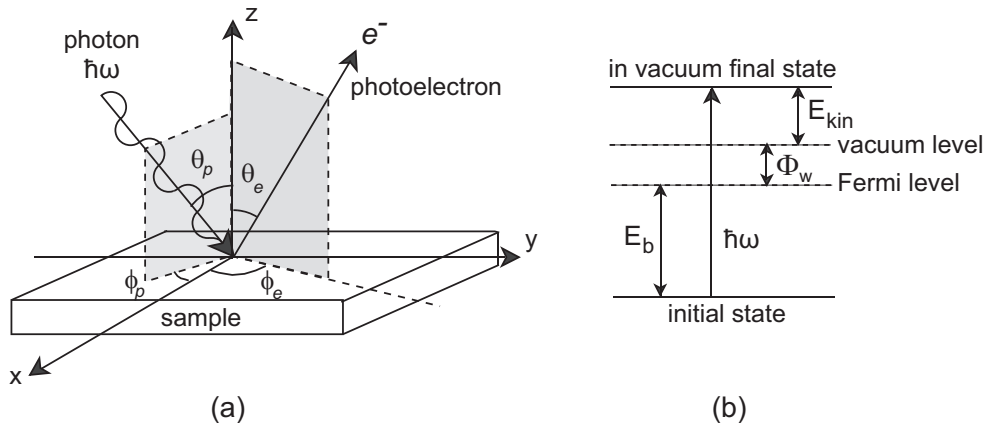

Figure 1: Schematic view of the photoemission process: (a) a photon of energy $\hbar\omega$ impinges on a solid surface, and after absorption of the photon an electron is ejected in a given direction (θ_e, ϕ_e) with respect to the reference system; (b) corresponding energy balance within the framework of a single particle (or one electron) picture. In (b) Φ_w denotes the work function of the material.

electron with binding energy E_B below the vacuum level: the entire photon energy is transferred to the electron, which is then promoted to an unoccupied state above the vacuum level. As a result, this *photoelectron* is ejected into the vacuum with kinetic energy:

$$E_{kin} = \hbar\omega - E_B \tag{1}$$

and can be detected by an electron energy analyzer.
For a solid surface the binding energy[1] (E_b) is conventionally measured with respect to the Fermi level rather than to the vacuum level (Fig. 1b), and the previous relationship is written in the form:

$$E_{kin} = \hbar\omega - E_b - \Phi_w \tag{2}$$

Here, Φ_w is the *work function* of the material and represents the minimum energy required to remove an electron from the solid; it can be seen as an energy barrier that electrons need to overcome in order to escape from the surface into the vacuum. Obviously, for an electron to be excited, the photon energy must be greater than E_b with the difference at least exceeding Φ_w.

In the simple *single particle picture* described above, which is based on a single electron being excited, it is clear that the energy distribution of photoemitted electrons should be a faithful replica of the electron states in the solid shifted up in energy by an amount $\hbar\omega$-Φ_w (see Fig. 2). In practice, it provides only a distorted replica of the electronic structure, complicated − for example − by the occurrence of multi-electron processes and by the fact that the probability of a photon being absorbed is not the same for all electron states. The ejected electrons can originate from core levels or from the occupied portion of the valence band (Fig. 2); in standard XPS, however, due to the relatively high photon energy (typically in the range between 100−200 eV and 2000 eV), the attention is predominantly focused on core level electrons.

Three main aspects of XPS deserve a special mention:

- **the elemental sensitivity**
- **the chemical state specificity**
- **the surface sensitivity**

[1] In the following we adopt the notation E_b for the binding energy when the Fermi level is taken as the reference level, whereas E_B is used when the binding energy is referenced against the vacuum level.

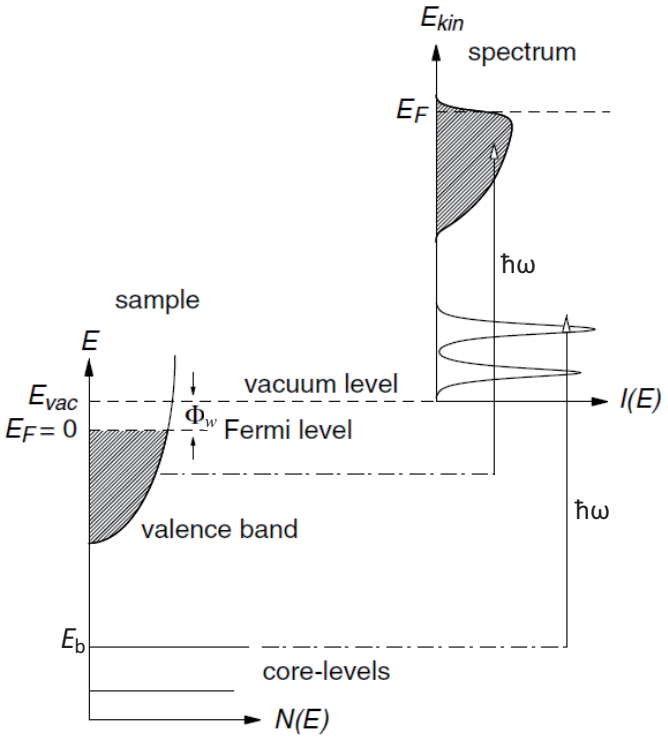

Figure 2: Schematic of the photoemission process in the single particle picture (adapted from Ref. [1]). Electrons with binding energy E_b can be excited above the vacuum level E_{vac} by photons with energy $\hbar\omega > E_b + \Phi_w$. The photoelectron distribution $I(E_{kin})$ can be measured by an electron energy analyzer and is - to a first approximation - a replica of $N(E_b)$, the occupied density of electronic states (DOS) in the sample.

1. A typical XPS spectrum is obtained at a given photon energy by recording the number of photoelectrons as a function of the kinetic energy and can be plotted as a function of the binding energy by making use of Eq. (2). The spectrum consists of a succession of distinct lines, reflecting the sequence of occupied levels - in particular the core levels - in the system under investigation. Since the binding energies of core levels are different for (and therefore characteristic of) each chemical element, and no two elements share the same set of binding energies, photoemission spectra can serve as "fingerprints" of the respective elements. For example, as illustrated in Fig. 3, a peak located at $E_b \sim 285$ eV is characteristic of photoelectrons coming from the C $1s$ core level, while the N $1s$ photoemission line appears at higher binding energy (~ 400 eV). This **elemental sensitivity** renders PES a very useful analytical tool, making it possible - for instance - to determine the composition of an unknown sample and to assess the degree of cleanliness of solid surfaces. Note that XPS can be used for analysis of all elements in the periodic table except hydrogen and helium.

2. When comparing the binding energies of core electrons of a given element in different systems (i.e., in different molecules, compounds or solids), one finds that the exact value of E_b depends on the chemical environment of the atoms and that energy shifts may occur when inequivalent atoms of the same elemental species are present (Fig. 4). These energy shifts are called *chemical shifts*. In general, electrons photoemitted from atoms in a higher positive oxidation state display a higher binding energy because of the increased Coulomb interaction with the ion core upon withdrawal of valence charge due to chemical bonding. By comparison with data from well-known "standard" substances, the values of the binding energy shifts can often be used to determine oxidation states and to gain insight into the nature of the chemical bond formed by the atoms. Such a **chemical state specificity**

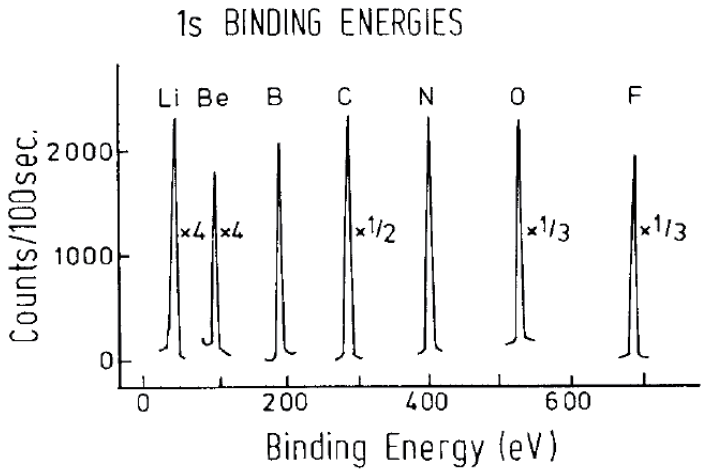

Figure 3: Photoemission spectra of the 1s core levels of the second row elements (taken from Ref. [2]).

is one of the major strengths of XPS for application in chemistry, surface physics and materials research, and is at the origin of the alternative name ESCA (Electron Spectroscopy for Chemical Analysis) with which the technique was originally denoted.

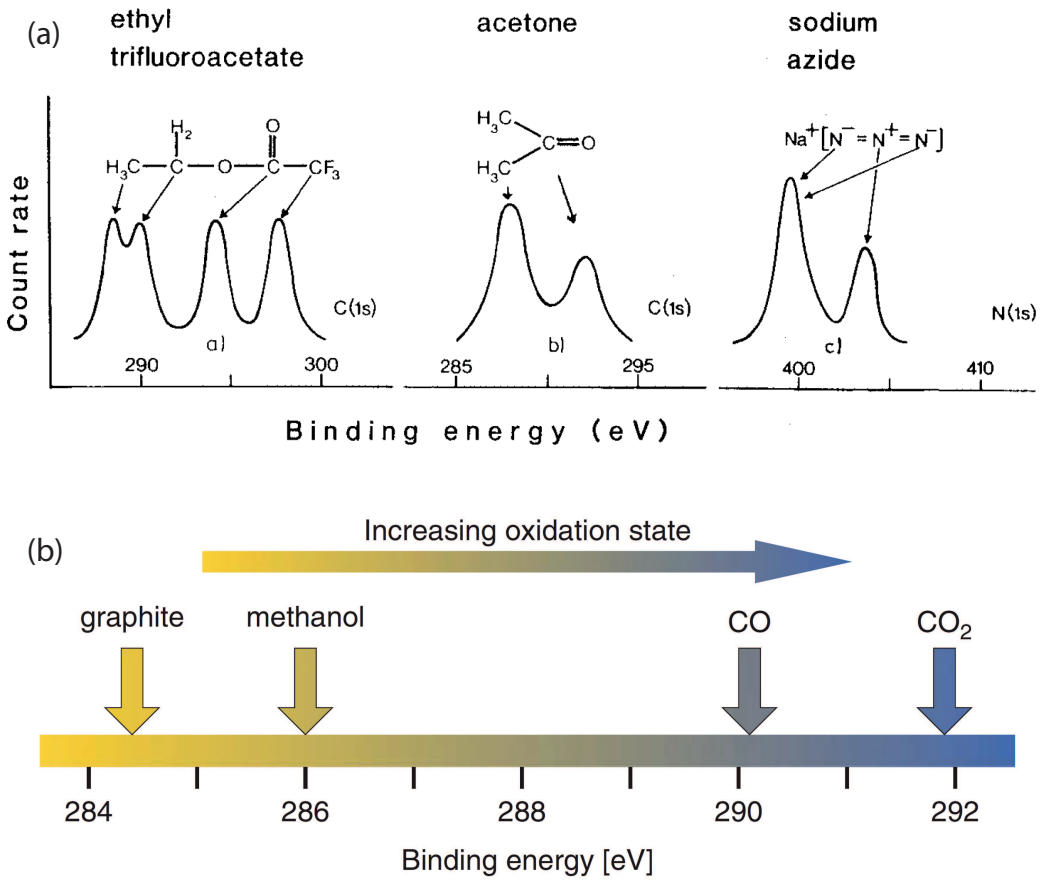

Figure 4: (a) Chemical shifts in isolated molecules (C 1s and N 1s levels; adapted from Ref. [2]). (b) A plot of the chemical shift in the C 1s binding energy in different carbon-containing compounds (from Ref. [3]).

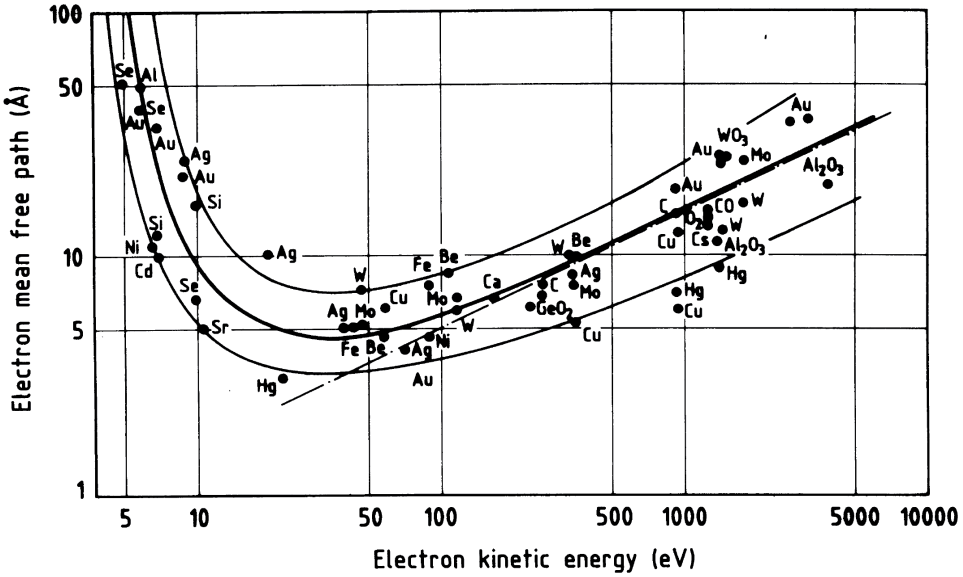

Figure 5: Inelastic mean free path of electrons as a function of their kinetic energy for various elements. While λ_e depends strongly on the kinetic energy, it is only weakly dependent on the material: for this reason the general trend $\lambda_e = \lambda_e(E_{kin})$ is often referred to as *universal curve*.

3. XPS and, more in general, all electron spectroscopies are highly **surface sensitive**, due to the strong interaction of electrons with matter. The latter entails that electrons travelling in a solid exhibit a very short inelastic mean free path, λ_e. This quantity describes the average distance that an electron can travel through the material without suffering energy losses by inelastic scattering; it therefore provides an indication of the electron escape depth. For electrons with kinetic energy in the range between 10 and 1000 eV, λ_e can vary between 5 and 30 Å depending on the material (Fig. 5) and thus amounts to only a few atomic layers. As a result, in a typical photoemission experiment only electrons originating from a narrow region at the solid-vacuum interface can reach the detector without losing energy, thus contributing to the main lines of the measured spectrum. For this reason, PES and XPS are widely employed to probe the electronic structure and composition of solid surfaces and thin films.

2.2 Beyond the single particle picture: binding energy and final state effects

The single particle picture adopted so far to describe the photoemission process assumes implicitly that when the photoelectron is excited above the vacuum level all other electrons in the sytem remain unperturbed in the same state as before the photoionization event. This assumption has an immediate implication on the location of a given core level peak, the binding energy of which should be simply equal to:

$$E_B(\nu) = E_f(N-1) - E_i(N) = -\epsilon_\nu \tag{3}$$

Here, $E_i(N)$ is the energy of the ground state of the atom with N electrons and $E_f(N-1)$ the energy of the final state of the ionized atom, whereas ϵ_ν denotes the energy of the electron in the state ν below the vacuum level. The previous expression, known as *Koopman's theorem*, is a consequence of the energy conservation $\hbar\omega + E_i(N) = E_{kin} + E_f(N-1)$ combined with Eq. (1).

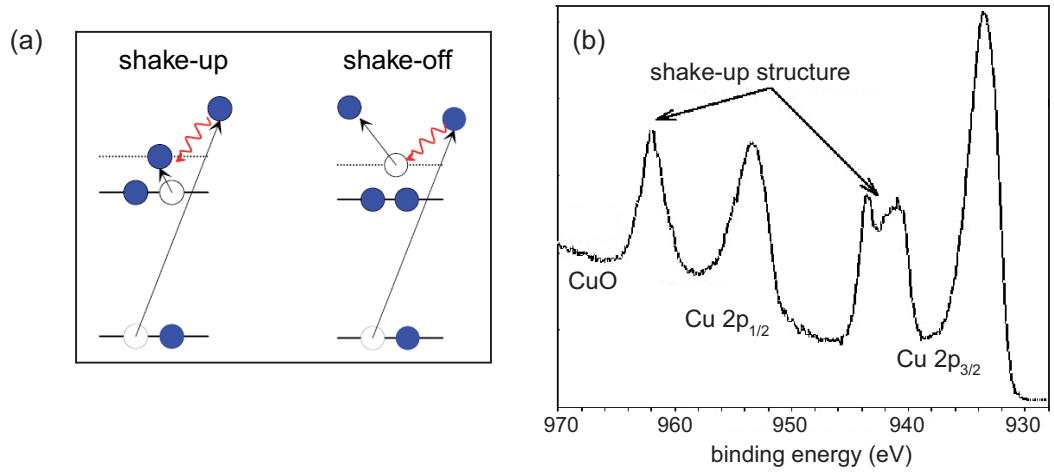

Figure 6: (a) Schematic of the shake-up and shake-off transitions; (b) Shake-up loss structure in the Cu 2*p* spectrum of copper (II) oxide (CuO), adapted from Ref. [5].

In reality, however, the Koopman's energy is never observed, and this can be mainly ascribed to the fact that the electron system "relaxes" in response to the creation of the vacancy in the inner shell (*core hole*) upon photoemission. This relaxation is an important many-body effect in the one-hole final state of the electron system. The core hole represents a positive charge acting on the remaining electrons, which rearrange themselves to partially shield the electron vacancy and to minimize the total energy of the ionized atom, thus making more energy available for the outgoing photoelectron. Therefore, the relaxation of the eletron system reduces the apparent binding energy E_B measured for the photoelectron. Typical relaxation shifts are of the order of 10-20 eV [4].

The screening of the core hole typically comprises an intra-atomic and an extra-atomic contribution. The former is due to the relaxation of the electrons (essentially, the outer shell electrons) of the excited atom itself and is the only contribution in isolated atoms. For atoms bound in molecules or solids the electrons of the neighboring atoms are also polarized by the creation of the core hole, although to a lesser extent, thus giving rise to the extra-atomic component of the relaxation. Because the screening of the core hole depends on the electronic environment[2], relaxations shifts differ from system to system for a specific core level line. This difference can contribute to the chemical shift described in §2.1, although in many cases the effect of the modified physical and chemical local environment on the initial electron state is considered to be dominant.

The relaxation of an electron system in response to the creation of a core hole is an important final state effect. Other final state effects that involve many-body processes and can lead to a modified photoelectron's kinetic energy are, for example, multi-electron excitations such as plasmon losses and *shake-up* and *shake-off* transitions. In all these processes, electronically excited final states are created upon photoemission, so that less kinetic energy is available for the photoelectron: this leads to satellite lines shifted to higher binding energy relative to the main core level line. Shake-up and shake-off satellites occur when an additional electron is promoted from an occupied energy level into a bound unoccupied state or into a state in the *continuum* above the vacuum level, respectively (Fig. 6). Plasmon loss satellites, instead, are the result of the excitation of quantized plasma oscillations, namely collective oscillations of the free electron gas density with respect to the positively charged ion cores. These plasmon satellites are displaced to higher binding energy relative to the "elastic" line by amounts $n(\hbar\omega_p) + m(\hbar\omega_s)$, where

[2]For example, the screening ensured by electron rearrangement is more effective in metals than in ionic solids, thanks to the presence of valence electrons (the *conduction electrons*) that are free to move inside the material. Accordingly, the magnitude of the relaxation shift is larger in metals than in ionic materials.

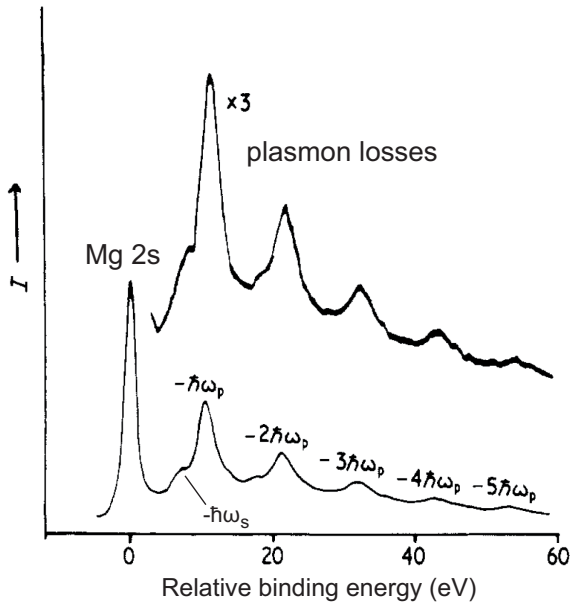

Figure 7: String of plasmon satellites in the Mg 2s XPS spectrum, adapted from Ref. [6].

n and m are integers and $\hbar\omega_p$ and $\hbar\omega_s$ are the energy of a bulk and a surface plasmon, respectively (Fig. 7).

2.3 Decay of a core hole

The ejection of an electron from an inner shell creates an electronically excited state with a core hole in that shell. This excited state can decay via two distinct de-excitation routes:

- The core hole is filled by an electron from an outer shell with simultaneous emission of a photon with energy equal to the difference in binding energy of the two levels involved in the electron transition. This is the well-known X-ray emission process or *X-ray fluorescence* (Fig. 8, path (a)).

- The core hole is filled by an electron from an outer shell as in the previous case, but the excess energy is transferred to another outer shell electron, which is emitted (Fig. 8, path (b)). The process, called *Auger decay*, involves three electrons: the electron knocked out in the initial photoionization event, the electron that decays to fill the inner shell vacancy, and the emitted electron from the outer shell (Auger electron). As a consequence, the final state is a doubly ionized state.
  Auger transitions are denoted with the notation XYZ, where X, Y and Z refer to the three shells involved in the decay process. For example, in a KLL transition the electron that leaves behind the initial core hole is from the K shell (1s state), while the other two electrons come from the L shell (2s or 2p levels).

X-ray fluorescence and Auger electron emission are competitive processes, the branching ratio of which is governed by the respective decay cross-sections. For the binding energy range below 1.5 keV, as in the present experiment, and especially for elements with low atomic number, the non-radiative decay by far prevails.

2.4 Linewidth of core level lines

The width and shape of a photoemission peak results from the convolution of different effects. One important contribution is related to instrumental factors, primarily the linewidth and lineshape of the X-ray line used for the excitation and the resolution of the

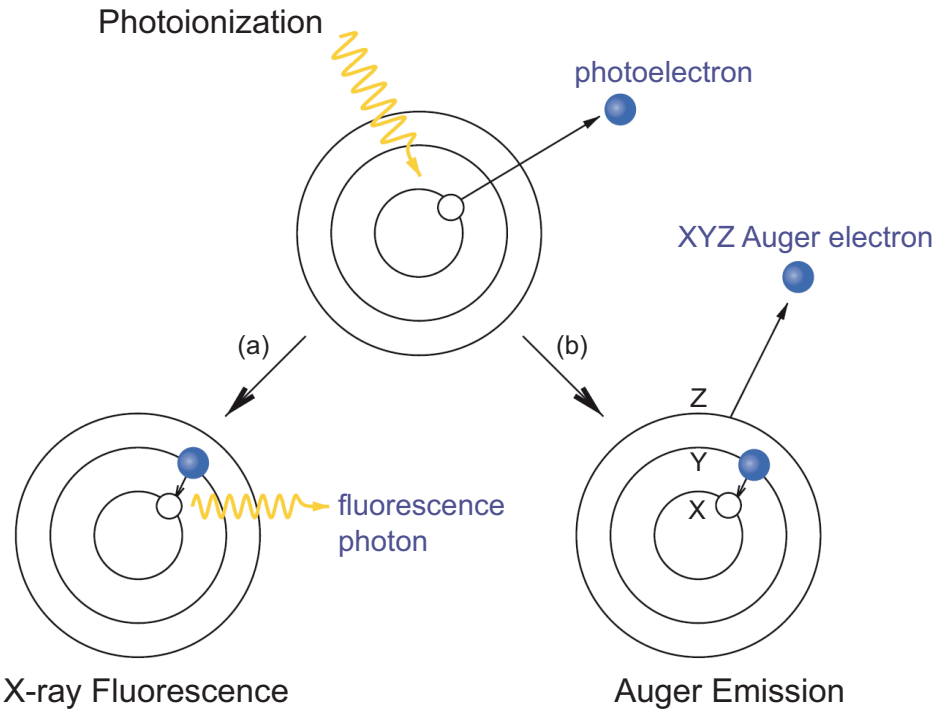

Figure 8: Schematic of (a) X-ray fluorescence and (b) Auger decay following a photoionization event. Adapted from Ref. [3].

electron energy analyzer employed to analyze in energy the distribution of photoelectrons. Another essential contribution, related to the photoemission process itself, is the peak broadening due to the finite lifetime of the core hole. Thermal braodening by coupling with intra-molecular vibrations and phonons may be non-negligible in some cases. In addition, many-body effects, such as the excitation of electron-hole pairs close to the Fermi level in metals or shake-up satellites that cannot be resolved due to limited instrumental resolution, can cause additional asymmetric broadening with a tail on the low kinetic energy side of the photoemission peak.

Instrumental and vibrational broadening yield Gaussian lineshapes. The spectral lineshape due to the core hole lifetime τ is instead a Lorentzian function with full-width at half-maximum (FWHM) 2Γ, the so-called *intrinsic* or *natural* linewidth, which is related to the mean lifetime through the relationship [7]:

$$2\Gamma = \frac{\hbar}{\tau} = \frac{6.58 \times 10^{-16}\ \text{eV} \cdot \text{sec}}{\tau\ [\text{sec}]} \tag{4}$$

2Γ is typically larger for inner shell orbitals, because these can be filled rapidly by electrons from the outer shells. Therefore, for a given element 2Γ tends to increase with increasing binding energy. In a similar way, for a given core level orbital (e.g., $1s$) 2Γ increases as the atomic number Z increases, due to the higher valence electron density in heavier atoms.

The contributions of intrinsic and instrumental effects to the experimentally observed linewidth can be combined to a first approximation into a quadratic sum [8]:

$$FWHM^2_{\text{tot}} = (2\Gamma)^2 \ + \ FWHM^2_X \ + \ FWHM^2_A \tag{5}$$

with the second and third term on the right side due to the X-ray source and analyzer energy resolution, respectively.

(a)

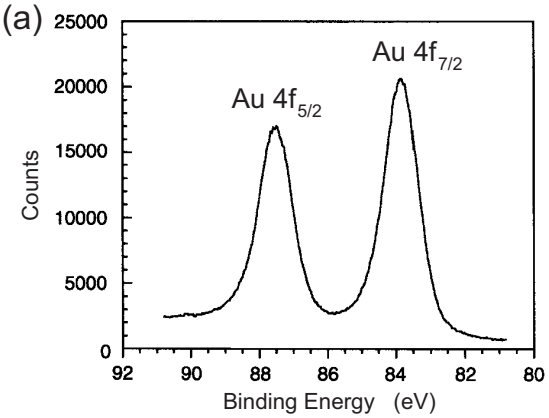

(b)

Subshell	Total angular momentum j components	Ratio of the degeneracies ($g = 2j + 1$)
s	1/2	-
p	3/2, 1/2	4/2
d	5/2, 3/2	6/4
f	7/2, 5/2	8/6

Figure 9: (a) Spin-orbit coupling leads to a splitting of the $4f$ photoemission line of gold into a doublet [2]. (b) Table listing spin-orbit split components and intensity ratios for different subshells. The notation $n[l\text{-subshell}]_j$ is commonly used (e.g., $4f_{7/2}$).

2.5 Spin-orbit splitting of core level lines

In the photoemission from p, d and f inner subshells the spectral lines are split into two-component peaks (Fig. 9a). This splitting arises from spin-orbit coupling effects in the final state [8]. While in the initial state the inner subshells are completely filled (for example, the configuration of the inner shells in gold is: $(1s)^2\ (2s)^2\ (2p)^6$ ... $(4f)^{14}$ ...), in the final state one electron has been removed and an unpaired spin is left behind. The spin can be oriented up or down, and if the core hole belongs to an orbital with non-zero orbital angular momentum ($l > 0$) there will be a coupling between the unpaired spin and the orbital angular momentum: the two states $j_+ = l + 1/2$ and $j_- = l - 1/2$ are not degenerate and a spin-orbit split doublet is observed in the photoelectron spectrum. The intensity ratio of the two spin-orbit components is dictated by the ratio of the respective multiplicities: $(2j_+ + 1)/(2j_- + 1) = (2l + 2)/2l$ (Fig. 9b), which determines the relative probability of transition to the two states upon photoionization. Generally, in the photoemission spectrum from a given subshell the core level subpeak with maximum j is detected at lower binding energy. Obviously, no spin-orbit splitting occurs in the photoemission from s core levels.

2.6 Summary – spectral features in a photoemission spectrum

We can now understand all the main spectral features that can be observed in a typical XPS spectrum of a solid (as the one illustrated in Fig. 10) and reflect the characteristic excitation processes in condensed matter.

As noted above, XPS spectra are in general dominated by sharp peaks corresponding to core level photoemission. These peaks may contain chemically shifted components and be spin-orbit split. Their binding energies always incorporate the contribution of the relaxation shift and their linewidth can be affected by many-body effects, instrumental resolution and natural broadening. In many cases, from the relative intensity of core level peaks one can estimate semi-quantitatively elemental ratios, in order to assess the relative surface coverage of adsorbates and contaminants or the stoichiometry of a compound. To this purpose it is necessary to correct the relative intensities by the respective photoionization cross-sections, which express the probability of creating a photoelectron in each core level at the photon energy $\hbar\omega$.

Together with core level lines, electron emission from the valence band is also observed. This part of the spectrum thus represents a projection of the occupied electronic states to energy above the vacuum level, and the photoemission intensity drops to zero above the

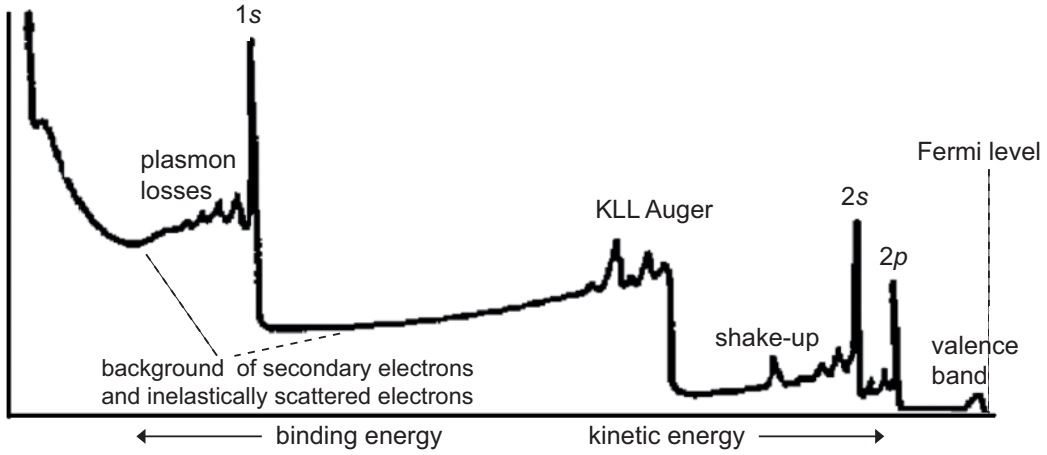

Figure 10: A typical XPS overview spectrum from a solid surface. Adapted from Ref. [9].

Fermi level (Fig. 10, right end of the spectrum).

Since Auger electrons are also detected by the electron energy analyzer, Auger lines are often observed. If it is possible to change the photon energy for the acquisition of the spectrum, an Auger line can be easily distinguished from a core level line, because the former appears at fixed kinetic energy regardelss of the photon energy, while the latter moves linearly with the photon energy according to Eq. (2).

Satellites corresponding to multi-electron excitations, such as multiple plasmon losses and shake-up satellites, may also show up in the XPS overview spectrum. Finally, if X-ray emission lines corresponding to different photon energies are used for the excitation, replicas of the same core level peak at different kinetic energy will be observed. Note that all photoemission features appear superimposed on a featureless background[3], arising from inelastically scattered electrons (which undergo energy losses before escaping from the surface) and secondary electrons excited in "cascade" processes.

2.7 Sampling depth of XPS and collection geometry

As anticipated in §2.1, the surface sensitivity of XPS stems from the short inelastic mean free path of electrons. While X-rays interact only weakly with matter and consequently can penetrate deeply into a solid (1000 nm or more at $\hbar\omega \sim 1$ keV), electrons with energy in the range 5-1500 eV readily lose energy by inelastic scattering. The XPS experiments are mainly concerned with the intensity of emitted photoelectrons that have suffered no energy losses: therefore, the XPS sampling depth refers to a characteristic length over which electrons can travel without undergoing inelastic scattering events. This quantity is the inelastic mean free path λ_e plotted in Fig. 5, which is defined as the average distance that an electron of given kinetic energy E_{kin} travels between two successive inelastic collisions [8]. In other terms, the probability that the electron travels a distance z through the solid without undergoing inelastic scattering can be written as an exponential decay:

$$P(z) \propto e^{-\frac{z}{\lambda_e}} \quad \Longrightarrow \quad < z >= \int zP(z)dz = \lambda_e$$

If one considers for simplicity the electrons emitted in the direction perpendicular to a solid surface, a small element of thickness dz at a distance z from the surface ($z = 0$

[3]For the correct determination of peak areas, peak positions and peak widths this background needs to substracted.

denotes the surface plane) will give a contribution dI to the measured intensity:

$$dI \propto e^{-\frac{z}{\lambda_e}}\, dz \tag{6}$$

The total intensity I coming from a thin film of thickness t right underneath the surface is obtained by integrating Eq. (6) between 0 and t, and it thus amounts to:

$$I = I_0\, [1 - e^{-t/\lambda_e}] \tag{7}$$

The sampling depth of the XPS experiment is often defined as $t = 3\lambda_e$, which means that 95% of the photoemission intensity of the core level line comes from the corresponding region ($3\lambda_e$ thick) below the surface [8].

When detecting photoelectrons emitted at an angle θ_e away from the surface normal (see Fig. 1a), one has to consider the effective path $z/\cos\theta_e$ of the electrons in the solid, and Eq. (6) becomes:

$$dI \propto \exp[-\frac{z}{\lambda_e \cdot \cos\theta_e}] \cdot dz \tag{8}$$

Hence, in grazing emission geometry the sampling depth is reduced to $3\lambda_e\cos\theta_e$ and the surface sensitivity of the measurements is strongly increased (e.g., $\theta_e \sim 80° \implies \cos\theta_e \sim 0.17$).

3 Adsorption on surfaces

The term "adsorption" indicates the process of trapping and binding of foreign species (atoms or molecules) onto a surface by condensation from the gas phase. The energy released in this process is called energy of adsorption U_{ads} or also binding energy (not to be confused with the binding energy in PES). The term "substrate" refers to the solid surface onto which adsorption occurs, while "adsorbate" is used to indicate the species that are adsorbed onto the substrate (Fig. 11). Adsorption can be associative (if a particle or molecule is adsorbed as a single unit) or dissociative (if the particle or molecule is dissociated upon adsorption), and moreover adsorption processes may be reversible or irreversible.

The reverse process, the removal of adsorbed species from the surface, is called "desorption". Desorption may be stimulated by heat (thermal desorption), by electrons (electron stimulated desorption), or by photons or ions (photon or ion stimulated desorption).

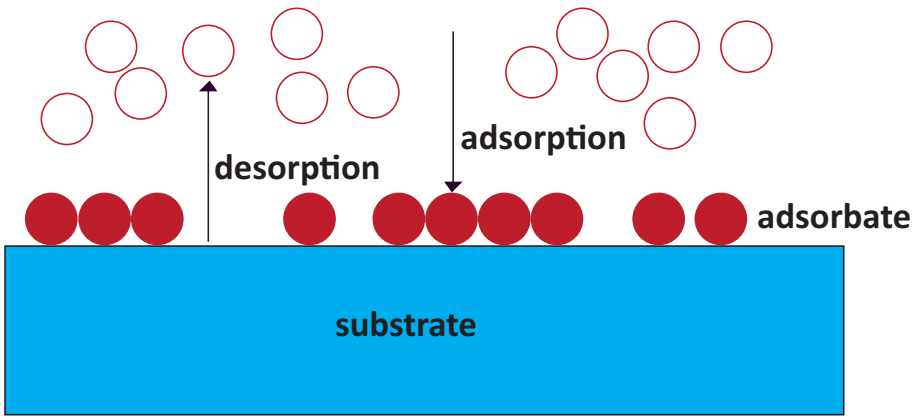

Figure 11: Schematic of adsorption onto (and desorption from) a solid surface.

3.1 Types of adsorption

Depending on the strength of the interaction between the adsorbate and the substrate, a distinction is typically made between two limiting cases:

- **Physisorption**
  Physical adsorption (= physisorption) is governed by weak Van der Waals interactions with the surface; no chemical bonds are formed. The adsorption energy U_{ads} is small, typically < 30 kJ/mol or 0.3 eV/particle. Formation of multilayers (condensates) is possible at sufficiently low temperatures.
  Example: He on noble metal surfaces at cryogenic temperatures.

- **Chemisorption**
  Chemical adsorption (= chemisorption) involves the formation of a chemical bond between the adsorbate and the surface, e.g. transfer of electrons and/or formation of covalent bonds (hybrid molecular orbitals). In most cases the adsorption energy is much larger than 30 kJ/mol, $\geq$ 100 kJ/mol or 1 eV/particle. Chemisorption is often dissociative and may be irreversible; activation barriers are possible, and chemisorbates form typically only a single layer (= direct contact of surface atoms and the chemisorbate is required). Moreover, specific binding sites may be favoured because of the highly corrugated surface potential.
  Examples: CO and oxygen chemisorption on transition metals at room temperature.

3.2 Adsorption order

- **First order adsorption**
  One particle from the gas phase yields one particle of the adsorbate, i.e., the impinging particles are molecules that do not dissociate upon adsorption. The reverse process is first order desorption.
  Examples: CO/nickel (CO chemisorbs on Ni surfaces molecularly with $U_{ads} \sim 120$ kJ/mole); Ar/Ruthenium (Ar physisorbs on Ru with $U_{ads} \sim 10$ kJ/mol).

- **Second order adsorption**
  A molecule dissociates upon adsorption. One particle in the gas phase yields two particles on the surface. The reverse process is second order (or associative) desorption.
  Example: H_2/Nickel (H_2 dissociates into two H atoms on Ni, $U_{ads} \sim 90$ kJ/mole).

3.3 Nomenclature

Other important concepts encountered in adsorption studies in the field of surface science:

- **Surface (relative) coverage Θ:** $\Theta \equiv \dfrac{N_{ads}}{N_{sub}}$
  with N_{ads} = number of adsorbate particles per unit area; N_{sub} = number of particles per unit area in the substrate surface layer. Θ is typically expressed in monolayers or as a fraction of monolayer (ML), 1 ML corresponding to an adsorbate surface density equal to the surface density of substrate atoms.

- **Collision rate ν:**
  it is defined as the number of particles hitting a surface per unit time and unit area. The Hertz-Knudsen equation following from the gas kinetic theory states that:

$$\nu = \frac{p}{\sqrt{2\pi M k_B T}} \qquad [\text{particles} \cdot \text{s}^{-1} \cdot \text{m}^{-2}]$$

  with p = pressure [N$\cdot$ m^{-2} = Pa]; M = particle mass [Kg]; T = temperature [K]; k_B = Boltzmann constant.

- **Sticking coefficient s:**

$$s = \frac{dN_{ads}}{dt} \Big/ \frac{dN_{coll}}{dt} \qquad\qquad 0 \leq s \leq 1$$

  probability that a particle colliding with the surface is adsorbed and stays on it.

- **Exposure:**
  measure of the amount of gas that a surface has been exposed to; more specifically, the product of the gas pressure and the time of exposure. Normal unit is the Langmuir, where $1L = 10^{-6}$ Torr ·s (1 Torr = 133.3 Pa = 1.333 mbar).

4 Experimental set-up

The set-up that will be used for the experiment is schematically depicted in Fig. 12 and is based on an ultra-high vacuum (UHV) chamber on which the XPS apparatus and all equipments for sample insertion, preparation and manipulation are mounted.

4.1 Vacuum system

The UHV chamber is maintained at a base pressure lower than 1×10^{-9} mbar (1×10^{-7} Pa). This low pressure is required in order to permit electron detection (avoiding scattering of

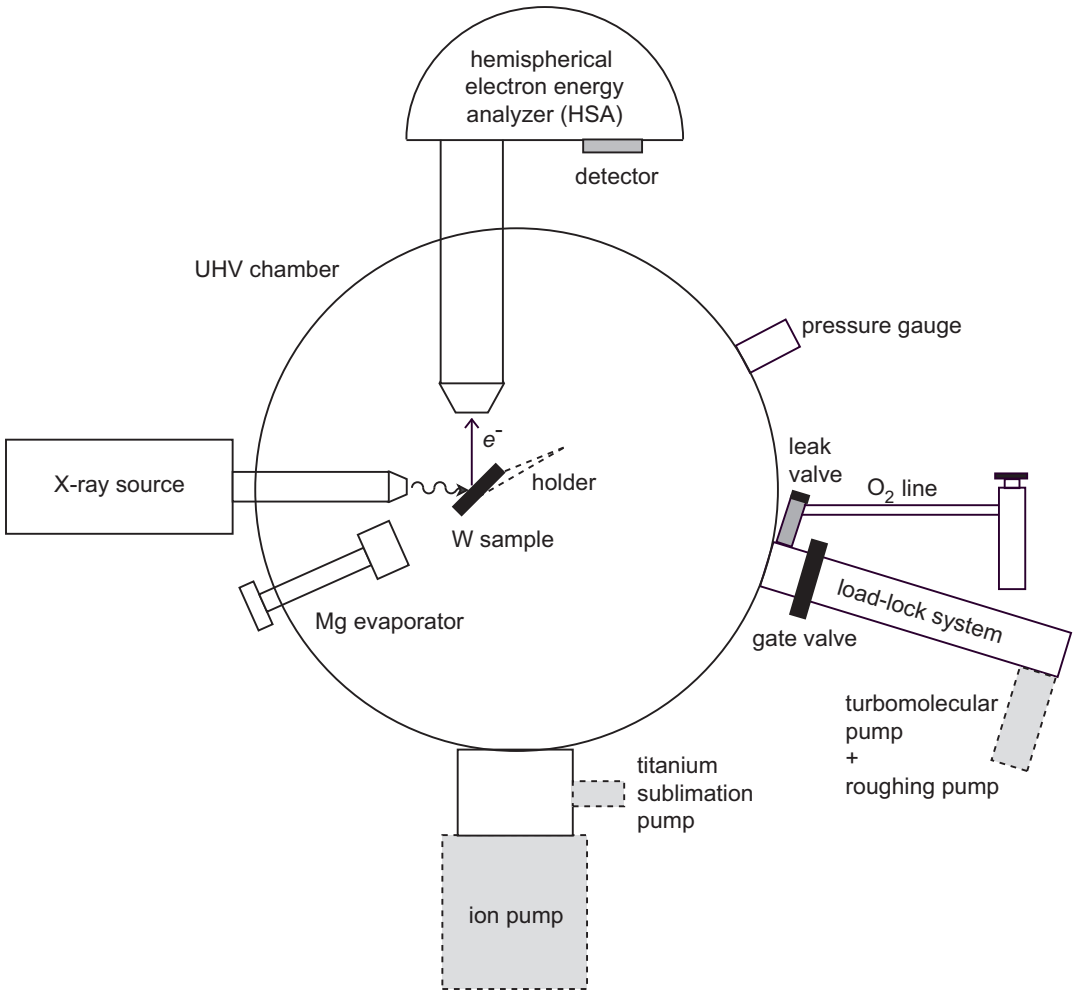

Figure 12: Scheme of the UHV chamber with the XPS apparatus and ancillary equipments.

the photoelectrons from residual gases between the sample surface and the detector) and to ensure that atomically clean surfaces can be prepared and maintained free of contaminants during the experiment. The chamber is pumped by an ion pump directly mounted inside the chamber. Auxiliary pumping by a titanium sublimation pump is possible. In addition, an external turbomolecular pump (with attached a backing roughing pump) can be connected to the UHV chamber through a gate valve. This turbomolecular pump is also used to pump the load-lock system adjacent to the main chamber. The UHV regime can only be reached after baking out the chamber for about 24 hours (or longer) at temperatures exceeding 160-180°C. This procedure allows to eliminate residual molecules (predominantly water) adsorbed on the stainless steel walls of the chamber, which otherwise would be released at a low rate thus increasing the pressure. A brief introduction to the UHV technology, instrumentation and related protocols can be found in Refs. [10, 11].

4.2 X-ray source

A conventional X-ray tube provides characteristic Al $K\alpha$ radiation. This photon source consists of a cathode filament, which emits electrons upon direct current heating (filament current: 4.5 A), and an anode, onto which the electrons are accelerated by applying a high voltage (11-12 kV). The typical emission current (i.e., the current of electrons leaving the cathode and reaching the anode) is 20-22 mA. Water cooling is required during continuous duty operation of the X-ray source, in order to prevent melting of the anode target. The anode is an Al film, some 10 μm thick, supported on a copper rod. During operation, the electrons from the cathode collide with the atoms of the Al target, causing vacancies in inner electron shells. The subsequent de-excitation by fluorescence decay (see §2.3) produces X-ray radiation of characteristic energy.

As illustrated in Fig. 13, the $K\alpha_1$ and $K\alpha_2$ lines are generated, corresponding to $L_3 \rightarrow K$ and $L_2 \rightarrow K$ transitions, respectively, where L_3, L_2 and K denote the $2p_{3/2}$, $2p_{1/2}$ and $1s$ levels. The $L_{2,3}$ subshell is split due to spin-orbit coupling in the final state, such that the relative intensity of the two lines reflects the L_3 to L_2 population ratio of 2 : 1. As a consequence, the $K\alpha_{1,2}$ line is in principle a doublet with an energy splitting of 0.43 eV. However, since each line has a natural width of 0.47 eV caused by lifetime broadening, the doublet cannot be resolved and the resulting composite line has

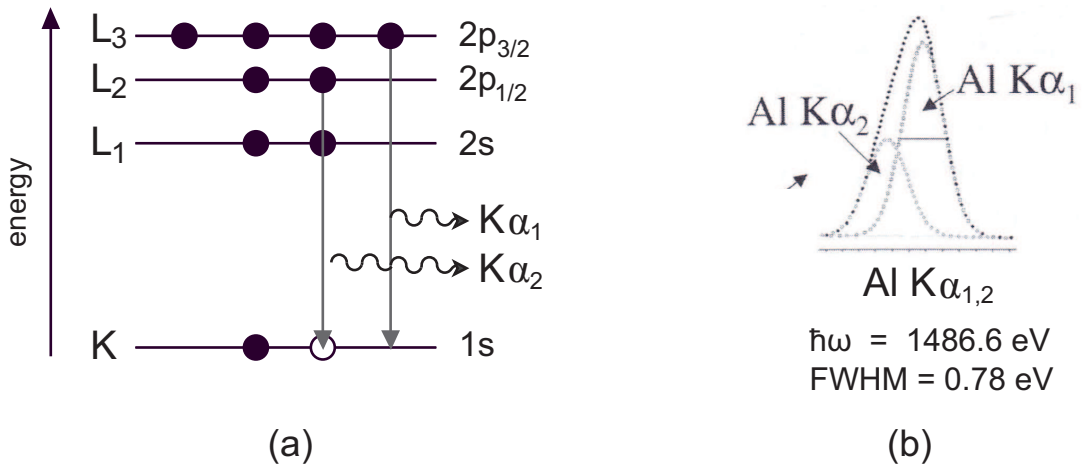

Figure 13: Characteristic radiation from an Al anode source: (a) schematic energy level diagram explaining the production of the individual $K\alpha_1$ and $K\alpha_2$ lines; (b) emission spectrum showing the convolution of the $K\alpha_1$ and $K\alpha_2$ lines into a composite $K\alpha_{1,2}$ line centered at 1486.6 eV with 0.78 eV FWHM. Adapted from Ref. [12].

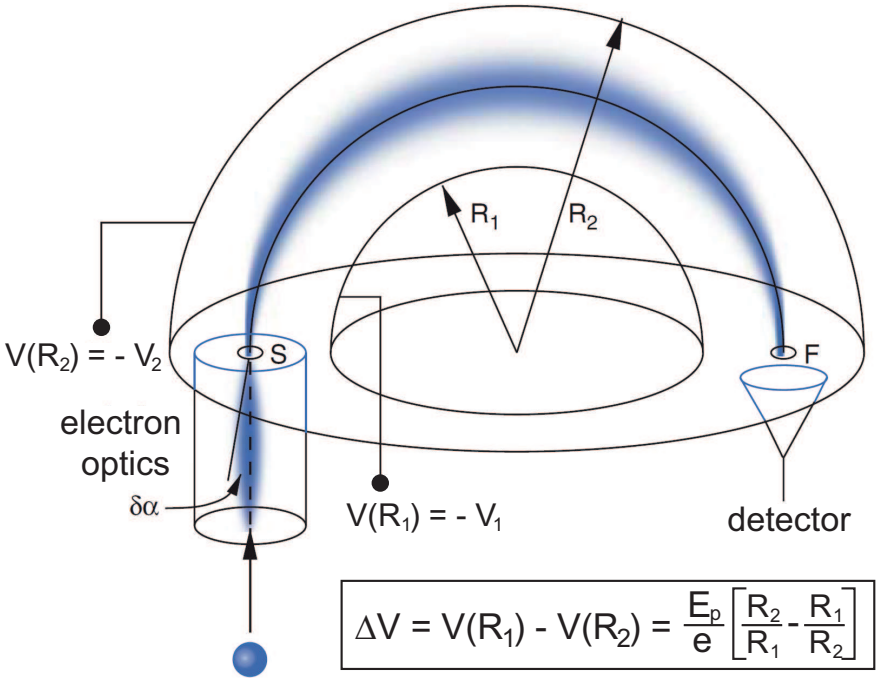

Figure 14: Schematic of a concentric hemispherical analyzer. Both hemispheres are at negative potential, with $V(R_2) < V(R_1)$ ($\rightarrow V_2 > V_1$). Adapted from Ref. [3].

a linewidth of 0.78 eV (FWHM) and is centered at $\hbar\omega = 1486.6$ eV. In addition, a $K\alpha_{3,4}$ satellite is also produced, attributed to emission from doubly ionized atoms [12]. This satellite line is centered at about 1496 eV and its intensity is $\sim 10\%$ of that of the main $K\alpha_{1,2}$ emission.

Additional emission lines can arise from contamination (e.g., the O $K\alpha$ line centered at $\hbar\omega = 524.9$ eV if the anode material is partly oxidized) or other modifications of the anode (e.g., when the Al film becomes too thin, the Cu L_α line from the copper rod beneath may be excited, $\hbar\omega = 929.7$ eV).

4.3 Electron energy analyzer

An electrostatic 180° hemispherical analyzer (HSA) is used to analyze in energy the electrons emitted from the sample. This electrostatic device, which consists of two metallic hemispheres concentrically arranged as in Fig. 14, enables to "disperse" the electrons as a function of their kinetic energy similarly to a prism that disperses light depending on its wavelength. For this purpose, a potential difference ΔV is applied between the inner and outer hemispheres, so that the trajectory of the incoming electrons is bent into a curve[4]. An electrostatic lens between the sample and the entrance slit S of the analyzer focuses the photoelectrons from the sample onto S. At a given ΔV, ideally only the electrons with a well-defined kinetic energy E_p are able to complete their path along the median trajectory of radius $R_0 = (R_1 + R_2)/2$ (where R_1 and R_2 are the radii of the inner and outer hemisphere, respectively) and emerge at the exit slit F. E_p is called *pass energy* and its typical values range between 5 and 50 eV for XPS measurements.

Importantly, the choice of the pass energy determine the *energy resolution* of the analyzer, which quantifies the ability to separate ($\rightarrow$ to *resolve*) peaks that differ in energy by only small amounts. The lower the pass energy, the better the resolving power. As discussed in §2.4, the energy resolution of the analyzer contributes to the overall FWHM

[4]To prevent perturbation of the electron trajectories by stray magnetic fields, the analyzer region is shielded by a μ-metal shield inside the vacuum vessel.

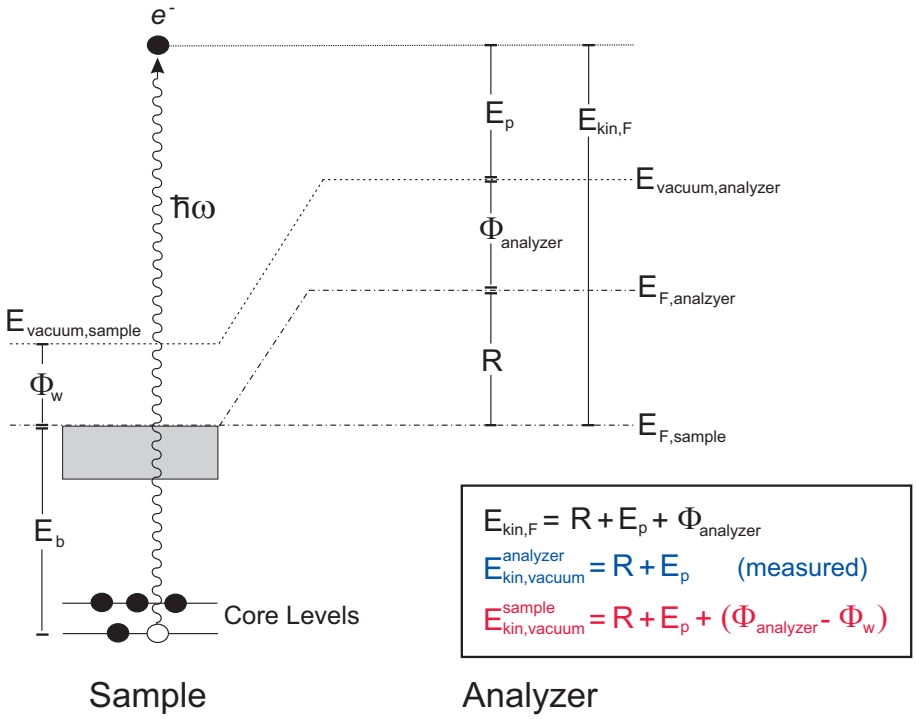

Figure 15: Photoelectron detection by an electron energy analyzer: schematic diagram of relevant energy levels and voltages.

of a core level peak (Eq. (5)). For the HSA the following expression holds [11, 12]:

$$\frac{\Delta E}{E_p} = \frac{W_S + W_F}{4R_0} + \frac{\alpha^2}{2} \tag{9}$$

in which ΔE is the FWHM contribution from the analyzer ($FWHM_A$), W_S and W_F are the widths of the entrance and exit slit, respectively, and α is the angular spread of the electron beam. During the XPS measurements, the analyzer is operated at constant pass energy to yield a constant absolute energy resolution ΔE.

In order to enable scans over arbitrary kinetic energy ranges, the electrons are retarded (or accelerated) to the kinetic energy E_p by a potential difference R inside the lens system between the sample and the entrance slit. A channel-type electron multiplier (*channeltron* detector) is situated behind the exit slit of the analyzer and counts the emerging electrons. Therefore, by scanning R one can record a spectrum of the photoelectron intensity as a function of the kinetic energy, the measured kinetic energy being simply $R + E_p$.

When $R = 0$, the Fermi levels of sample and analyzer are aligned (in practice, both objects are grounded), whereas they are separated by R when the retarding voltage is applied. However, due to the different values of the work function, the vacuum levels of sample and analyzer do not coincide even for $R = 0$. From the energy level diagram illustrated in Fig. 15 it then follows that:

$$E_b = \hbar\omega - (E_p - \Phi_{\text{analyzer}} - R) = \hbar\omega - E^{\text{analyzer}}_{\text{kin, vacuum}} - \Phi_{\text{analyzer}} \tag{10}$$

Eq. (10) shows that the work function of the analyzer, rather than the work function of the sample, needs to be taken into account for calibrating the binding energy scale. Φ_{analyzer} enters the equation because in the experiment the kinetic energy scale is referenced to the vacuum level of the analyzer. To keep Φ_{analyzer} constant, all electrodes are covered with a chemically inert material (gold or graphite; in the present case graphite).

4.4 Samples

Four samples will be investigated during the experiment. Initially, a tungsten (W) ribbon will be studied. It can be heated up to 2500 K by direct current flow, in order to remove contamination from the surface. The W ribbon is mounted on a four-degree-of-freedom manipulator enabling translational motion along three orthogonal directions and rotation around the axis of the manipulator. In this way, the polar angle θ_e between the electron emission direction and the surface normal (see also Fig. 1a) can be changed - ideally - between 0° and 90°, thus controlling the surface sensitivity of the XPS measurements.

Further, the W ribbon will serve as substrate for the growth of a relatively thick Mg film that will be deposited *in-situ* under UHV conditions. Here, Auger electron emission from the KLL decay will enable to study the excitation of plasmons in the metal film. Moreover, the subsequent oxidation of magnesium at room temperature will provide a clear illustration of the concept of chemical shift and of the information that can be gained by changing the surface sensitivity.

Additional samples can be introduced through the custom-made load-lock system (Fig. 12). This system allows fast insertion of *ex-situ* prepared samples without breaking the vacuum of the main chamber. For example, a gold substrate covered by an organic self-assembled monolayer (SAM) could be investigated. The SAM is prepared by immersion of the substrate into an ethanol solution containing thiol molecules. Thiols are endowed with a SH functional group, which provides a strong anchoring to gold upon breaking of the S-H bond. Alternatively, a sample of carbon nanotube powders or a graphite substrate covered by organic molecules (such as metalloporphyrins or metal phthalocyanines) could be studied. The elemental and chemical state analysis will provide valuable insight into the composition of the system, nature of the adsorbed molecules, bonding interactions etc.

4.5 Magnesium evaporator

The evaporator consists of a small high-melting-point crucible containing Mg grains. The crucible is heated by passing current through a conducting wire coiled around it. Prior to evaporation, the Mg grains need to be outgassed repeatedly, in order to ensure that a clean Mg film is deposited onto the tungsten ribbon during the experiment.

4.6 Gas handling line

A gas line filled with molecular oxygen is connected to the main chamber through a high-precision leak valve. In this way, O_2 can be admitted into the chamber in a controllable fashion during the experiment.

5 Important concepts

The following concepts should be clear before coming to the experiment:

- Fundamental principles of XPS. Photoelectrons and Auger electrons. Core level lines. Binding energy and work function. Spin-orbit splitting. Chemical shifts.
- Surface sensitivity of XPS. Importance of the electron detection geometry.
- Operating principle of the X-ray tube. Emission lines from the Al anode.
- Hemispherical electron energy analyzer. Pass energy and retarding voltage. Energy resolution.

6 Instructions for the experimental session

The goal of the experiment is to learn how to use XPS for **elemental** and **chemical analysis**. Insight into instrumentation, methodology for data acquisition and interpretation of the results will be provided. After getting an introduction to the experiment and the equipments by the advisor you will follow the four steps (A-C) listed below.

A. Performance of the analyzer and characterization of the W sample

The advisor will show how to clean the W ribbon and you will repeat the operation twice. Afterwards, the sample can be brought into the measurement position. Turn it in order to have an electron emission angle of 45° (this also corresponds to a 45° incidence angle of the photon beam relative to the surface normal). The advisor will explain the operations for switching on the X-ray source (high voltage: 12 kV) and the HSA analyzer, and you will learn how to run measurements via computer. Importantly, make sure that you have set the correct value of the pass energy before each measurement. Acquire the following scans, while simultaneously doing the data analysis to understand what you are measuring:

1. Take an **overview scan** with 100 eV $\leq E_{\text{kin}} \leq$ 1500 eV (energy step: 1 eV). Since you are not interested in the fine details of this wide scan, you can set $E_p = 50$ eV ($\rightarrow$ low energy resolution). Repeat the scan until a good statistics is obtained. If needed, you can sum all scans using an appropriate computer software.

2. Try to **assign all maxima** in the previous spectrum to known core level and Auger peaks: this may be easier if you plot the spectrum in the binding energy scale, using the appropriate computer software (for the moment just use a reasonable value for the analyzer work function).

3. **Zoom-in** into the W $4f$ core level region, using an energy step of 0.1 eV. Record a sequence of spectra with different values of E_p (e.g., 7.5, 10, 15, 20, and 50 eV). In order to have good statistics, at each value of the pass energy select appropriately the integration time per energy point. Observe the effect of the pass energy on the analyzer resolution. In which situation is the spin-orbit splitting clearer?

4. Analyzing the previous data with the computer software, **estimate the FWHM** of the W $4f_{7/2}$ component and plot it as a function of E_p. Which trend do you observe (e.g., parabolic, linear etc.)? Does it appear reasonable to you?

5. Consider the W $4f$ spectrum at $E_p = 10$ eV and look for the tabulated binding energy of the W $4f_{7/2}$ component in polycrystalline tungsten. Can you now determine the **work function** of the analyzer?

6. **Zoom-in** into the C $1s$ and O$1s$ core level regions at E_p=50 eV. Is the surface completely free of contaminants?

B. Deposition of the Mg metal film

With the help of the advisor you will now deposit a Mg film onto the W ribbon, with the latter held at room temperature. You can monitor the change of pressure in the chamber during the deposition. Proceed according to the following instructions:

7. Record an **overview scan** from 50 to 1500 eV ($\theta_e = 45°$, $E_p = 50$ eV, $\Delta E_{\text{step}} = 1$ eV). Assign all the features of this spectrum and assess qualitatively the cleanliness and thickness of the film. Can you see any signal from the W substrate? Taking into account the inelastic mean free path of electrons and the collection geometry give a lower limit for the thickness.

8. Record the Mg KLL **Auger spectrum** in the kinetic energy range from 1060 eV to 1200 eV ($E_p = 20$ eV, $\Delta E_{\rm step} \sim 0.2 - 0.3$ eV) for:
(1) nearly normal electron exit ($\theta_e = 10°$);
(2) nearly grazing electron exit ($\theta_e = 80°$).
Keeping in mind the different probing depth of the two geometries, can you conclude that the (electronic) structure of the metallic film is uniform across its thickness?

9. Take a closer look at the previous spectra and with the help of the literature (e.g., Refs. [6, 13]) identify the features related to plasmon excitations. Determine the **plasmon energy**.

10. **Zoom-in** into the Mg 1s region ($\theta_e = 45°$, $E_p = 10$ eV, $\Delta E_{\rm step} = 0.1$ eV). Write down the kinetic energy of the main line. Record a photoemission spectrum ($E_p = 10$ eV) from the O 1s region. Is the metal film oxygen-free?

C. Oxidation of the Mg film at room temperature

You will help the advisor to oxidize the Mg overlayer at room temperature, letting O_2 into the chamber ($p = 2 \times 10^{-7}$ mbar) for about 5 minutes. Check that the pressure remains constant during this time and estimate the total exposure in Langmuir.

11. **Zoom-in** into the Mg 1s and O 1s regions, as done previously. Do you observe any change in the position of the Mg 1s line upon oxidation? Explain the results in the light of what you have learnt about the chemical shift.

12. Monitor the changes in the **Auger spectra** at $\theta_e = 10°$ and 80°. Which conclusions can be drawn based on the different surface sensitivity of the two collection geometries? Try to understand whether the film is uniformly oxidized and structurally homogeneous across its thickness, or instead the surface region is different from the inner part of the film.

7 Drafting your report

Write a short but exhaustive report of your experiment. After a very concise introduction on the XPS technique and instrumentation, discuss the experimental results addressing the issues listed below. Note that all photoemission spectra should be plotted in the binding energy scale, whereas the Auger spectra can be kept in the kinetic energy scale.

A1. Assess the cleanliness of the W ribbon and assign all features of the overview scan. Focus your attention on the W 4f doublet, give an estimate of the analyzer work function and discuss the effect of the pass energy on the resolution, plotting the experimentally obtained FWHMs for the $4f_{7/2}$ component as a function of E_p. Explain the spin-orbit splitting and for the case E_p=10 eV compare the intensity ratio of the two spin-orbit components with the expected branching ratio. Finally, from the experimental FHWM determine a lower limit for the lifetime of the $4f_{7/2}$ core hole by making use of Eqs. (4) and (5).

B1. Assign all features in the overview spectrum of the pristine Mg film. Consider the plasmon loss progression in the Auger KLL spectra. Compare the value you have determined for the bulk plasmon energy (in eV) with the predicted one in the free electron model: $\hbar\omega_p = [n\hbar^2 e^2/m_e\epsilon_0]^{1/2}$, with m_e electron mass and n conduction electron density. From the mass density and atomic weight of Mg and assuming two conduction electrons per atom, justify that $n_{\rm Mg} \simeq 8.6 \times 10^{28}$ electrons/m^3.

B2. By consulting available literature (e.g., Refs.[6, 13]), identify the main transitions in the Auger spectra ($KL_{2,3}L_{2,3}$, KL_1L_1 etc.). You may also check the reliability of the work function value determined above by comparing the tabulated and experimental values for the intense KL_2L_3 ($^1D_2$) line[5].

B3. By comparing the Auger spectra in different collection geometries comment on the thickness of the metallic Mg film and make conclusions on its uniformity.

C1. Compare the Mg 1*s* and O 1*s* spectra before and after oxidation, showing each region on the same plot. Describe the effect of the oxidation (structural and chemical evolution) by commenting on binding energy values and chemical shift.

C2. Is the Mg film uniformly oxidized through its thickness or can you infer differences between the surface layer(s) and the region underneath?

8 Useful tables

- Electron binding energies for all elements:
  http://xdb.lbl.gov/Section1/Table_1-1.pdf
- Energies of the X-ray emission lines for all elements:
  http://xdb.lbl.gov/Section1/Table_1-2.pdf
- Subshell photoionization cross-sections:
  http://xdb.lbl.gov/Section1/Sec_1-5.pdf

References

[1] F. Reinert and S. Hüfner, *Photoemission Spectroscopy − from Early Days to Recent Applications*, New Journal of Physics **7**, 97 (2005); doi:10.1088/1367-2630/7/1/097.

[2] S. Hüfner, *Photelectron Spectroscopy — Principles and Applications*, Springer-Verlag, Berlin, 2003.

[3] P. Willmott, *An Introduction to Synchrotron Radiation — Techniques and Applications*, J. Wiley & Sons Ltd., 2011.

[4] D. P. Woodruff and T. A. Delchar, *Modern Techniques of Surface Science*, Cambridge University Press, 1994.

[5] M. C. Biesinger et al., *Resolving Surface Chemical States in XPS Analysis of First Row Transition Metals, Oxides and Hydroxides: Sc, Ti, V, Cu and Zn*, Applied Surface Science **257**, 887 (2010); doi:10.1016/j.apsusc.2010.07.086.

[6] J. C. Fuggle et al., *X-ray Excited Auger and Photoelectron Spectra of Magnesium, Some Alloys of Magnesium and its Oxide*, Journal of Physics F: Metal Physics **5**, 375 (1975); doi:10.1088/0305-4608/5/2/020.

[7] J. J. Sakurai, *Modern Quantum Mechanics*, Addison-Wesley Publishing Company, Reading - Massachusetts, 1995. See pp. 341-345.

[8] B. D. Ratner and D. G. Castner, *Electron Spectroscopy for Chemical Analysis* (Chapter 4), in: *Surface Analysis — The Principal Techniques*, edited by J. C. Vickerman, J. Wiley & Sons Ltd., 1997.

[5]Note that tabulated values are often given with the kinetic energy measured relative to the Fermi level.

[9] M. Henzler and W. Göpel, *Oberflächenphysik des Festkörpers*, Teubner Studienbücher, Stuttgart, 1994.

[10] K. Oura, V. G. Lifshits, A. A. Saranin, A. V. Zotov and M. Katayama, *Surface Science — An Introduction*, Springer-Verlag, Berlin, 2010. Chapter 3.

[11] J. C. Rivière, *Instrumentation* (Chapter 1), in: *PRACTICAL SURFACE ANALYSIS, Vol. 1: Auger and X-ray Photoelectron Spectroscopy*, edited by D. Briggs and M. P. Seah, J. Wiley & Sons Ltd., 1990.

[12] I. W. Drummond, *XPS: Instrumentation and Performance* (Chapter 5), in: *SURFACE ANALYSIS by Auger and X-ray Photoelectron Spectroscopy*, edited by D. Briggs and J. T. Grant, IM Publications and SurfaceSpectra Limited, 2003.

[13] P. Steiner et al., *The KLL Auger Spectra of Na and Mg Metal and Their Plasmon Structure*, Physica Status Solidi (b) **90**, 45 (1978); doi:10.1002/pssb.2220900104.